Research Article | Vol. 24, No. 14 | 11 Jul 2016 | OPTICS EXPRESS 15954

Optics EXPRESS

Nematic liquid crystal reorientation around multi-walled carbon nanotubes mapped via Raman microscopy

T. CACACE,[1,2,*] A. GARCÍA-GARCÍA,[3] G. ZITO,[2] V. TKACHENKO,[1,2] G. RUSCIANO,[2,4] M. A. GEDAY,[3] J.M. OTÓN,[3] A. MARINO[1,3] AND A. SASSO[2,4]

[1]*Institute of Applied Sciences and Intelligent Systems (CNRISASI), Via Campi Flegrei 34, I-80078, Pozzuoli (NA), Italy*
[2]*Physics Department "E. Pancini", University of Naples Federico II, Via Cinthia Monte S. Angelo, I-80126, Naples, Italy*
[3]*CEMDATIC, E.T.S.I. Telecomunicación, Polytechnic University of Madrid, Av. Complutense 30, E-28040 Madrid, Spain*
[4]*National Institute of Optics (INO)-National Research Council (CNR), Via Campi Flegrei 34, I-80078, Pozzuoli (NA), Italy*
[*]*t.cacace@isasi.cnr.it*

Abstract: We have studied the formation of topological defects in liquid crystal (LC) matrices induced by multiwalled carbon nanotubes (MWCNTs) and external electric fields. The defects are ascribable to a distortion of the LC molecular director in proximity of the MWCNT surface. The system is analyzed macroscopically using spectroscopic variable angle ellipsometry. Concurrently, confocal micro-Raman spectroscopy is used to study the system state at the microscale. This allows to acquire a three-dimensional, spatially-resolved map of the topological defect, determining scale length variations and orientation topography of the LC molecules around the MWCNT.

OCIS codes: (160.3710) Liquid crystals; (260.2130) Ellipsometry and polarimetry; (300.6450) Spectroscopy, Raman; (170.6900) Three-dimensional microscopy.

References and links

1. R. Saito, G. Dresselhaus, and M. S. Dresselhaus, *Physical Properties of Carbon Nanotubes* (Imperial College, 1998).
2. J. Beeckman, K. Neyts, and P. J. M. Vanbrabant, "Liquid-crystal photonic applications," Opt. Eng. **50**(8), 081202 (2011).
3. J. I. Sohn, W. K. Hong, S. S. Choi, H. J. Coles, M. E. Welland, S. N. Cha, and J. M. Kim, "Emerging applications of liquid crystals based on nanotechnology," Materials (Basel) **7**(3), 2044–2061 (2014).
4. G. Zito, B. Piccirillo, E. Santamato, A. Marino, V. Tkachenko, and G. Abbate, "Two-dimensional photonic quasicrystals by single beam computer-generated holography," Opt. Express **16**(8), 5164–5170 (2008).
5. G. Zito and S. Pissadakis, "Holographic polymer-dispersed liquid crystal Bragg grating integrated inside a solid core photonic crystal fiber," Opt. Lett. **38**(17), 3253–3256 (2013).
6. P. G. de Gennes and J. Prost, *The physics of Liquid Crystals* (Clarendon Press, 1995).
7. M. D. Lynch and D. L. Patrick, "Organizing carbon nanotubes with liquid crystals," Nano Lett. **2**(11), 1197–1201 (2002).
8. I. Dierking, G. Scalia, P. Morales, and D. LeClere, "Aligning and Reorienting Carbon Nanotubes with Nematic Liquid Crystals," Adv. Mater. **16**(11), 865–869 (2004).
9. I. Dierking, G. Scalia, and P. Morales, "Liquid crystal-carbon nanotube dispersions," J. Appl. Phys. **97**(4), 044309 (2005).
10. M. K. Massey, D. Volpati, F. Qaiser, A. Kotsialos, C. Pearson, D. A. Zeze, and M. C. Petty, "Alignment of liquid crystal/carbon nanotube dispersions for application in unconventional computing," AIP Conf. Proc. **1648**, 280009 (2015).
11. K. A. Park, S. M. Lee, S. H. Lee, and Y. H. Lee, "Anchoring a Liquid Crystal Molecule on a Single-Walled Carbon Nanotube," J. Phys. Chem. C **111**(4), 1620–1624 (2007).
12. S. J. Jeong, P. Sureshkumar, K.-U. Jeong, A. K. Srivastava, S. H. Lee, S. H. Jeong, Y. H. Lee, R. Lu, and S.-T. Wu, "Unusual double four-lobe textures generated by the motion of carbon nanotubes in a nematic liquid crystal," Opt. Express **15**(18), 11698–11705 (2007).

#263208 http://dx.doi.org/10.1364/OE.24.015954
Journal © 2016 Received 26 Apr 2016; revised 18 Jun 2016; accepted 20 Jun 2016; published 7 Jul 2016

Optics EXPRESS

13. R. Basu and G. S. Iannacchione, "Orientational coupling enhancement in a carbon nanotube dispersed liquid crystal," Phys. Rev. E Stat. Nonlin. Soft Matter Phys. **81**(5), 051705 (2010).
14. R. Basu, K. A. Boccuzzi, S. Ferjani, and C. Rosenblatt, "Carbon nanotube-induced chirality in an achiral liquid crystal," Appl. Phys. Lett. **97**(12), 121908 (2010).
15. I. Dierking, K. Casson, and R. Hampson, "Reorientation dynamics of liquid crystal-nanotube dispersions," Jpn. J. Appl. Phys. **47**(8), 6390–6393 (2008).
16. A. García-García, R. Vergaz, J. F. Algorri, X. Quintana, and J. M. Otón, "Electrical response of liquid crystal cells doped with multi-walled carbon nanotubes," Beilstein J. Nanotechnol. **6**, 396–403 (2015).
17. A. García-García, R. Vergaz, J. F. Algorri, G. Zito, T. Cacace, A. Marino, J. M. Otón, and M. A. Geday, "Reorientation of single-wall carbon nanotubes in negative anisotropy liquid crystals by an electric field," Beilstein J. Nanotechnol. **7**, 825–833 (2016).
18. V. Tkachenko, G. Abbate, A. Marino, F. Vita, M. Giocondo, A. Mazzulla, and L. De Stefano, "High accuracy optical characterization of anisotropic liquids by merging standard techniques," Appl. Phys. Lett. **89**(22), 221110 (2006).
19. A. Marino, V. Tkachenko, E. Santamato, N. Bennis, X. Quintana, J. M. Otón, and G. Abbate, "Measuring liquid crystal anchoring energy strength by spectroscopic ellipsometry," J. Appl. Phys. **107**(7), 073109 (2010).
20. A. C. De Luca, G. Rusciano, G. Pesce, S. Caserta, S. Guido, and A. Sasso, "Diffusion in polymer blends by Raman microscopy," Macromolecules **41**(15), 5512–5514 (2008).
21. M. Castriota, A. Fasanella, E. Cazzanelli, L. De Sio, R. Caputo, and C. Umeton, "In situ polarized micro-Raman investigation of periodic structures realized in liquid-crystalline composite materials," Opt. Express **19**(11), 10494–10500 (2011).
22. B. G. Saar, H. S. Park, X. S. Xie, and O. D. Lavrentovich, "Three-dimensional imaging of chemical bond orientation in liquid crystals by coherent anti- Stokes Raman scattering microscopy," Opt. Express **15**(21), 13585–13596 (2007).
23. S. Schymura and G. Scalia, "On the effect of carbon nanotubes on properties of liquid crystals," Phil. Trans. R. Soc. A **371,** 20120261 (2013).
24. G. Zito, G. Rusciano, G. Pesce, A. Dochshanov, and A. Sasso, "Surface-enhanced Raman imaging of cell membrane by a highly homogeneous and isotropic silver nanostructure," Nanoscale **7**(18), 8593–8606 (2015).

1. Introduction

Carbon nanotubes (CNTs) and liquid crystals (LCs) are intriguing materials. The former are highly anisotropic nanoparticles, easily visualized as rolled-up graphene sheets. CNTs are usually categorized in single-walled carbon nanotube (SWCNTs), with a single cylindrical wall, and multi-walled carbon nanotubes (MWCNTs), with multiple rolled concentric layers. Their exceptionally high aspect ratio leads to a large mechanical and electrical anisotropy [1].

Liquid crystals are anisotropic fluids, with intermediate properties between isotropic liquids and crystals. They are especially renowned for their leading role in the development of display technology, but their variety of uses is much wider, ranging from photonic devices (optical filters and switches, beam-steering devices, spatial light modulators), to lasers, sensors, integrated nanocomposite materials and many more [2–5]. In particular, thermotropic, calamitic (rod-like) LCs are extensively used in such applications. Liquid crystals exhibit a variety of phases, with different order degrees. In the nematic phase, the molecular centers of mass are randomly distributed; the anisotropy arises from orientational order: the rod-shaped LC molecules align spontaneously parallel to each other. The average direction chosen by the molecular long axes is known as molecular director $\boldsymbol{n}$ [6].

It has been observed that the LC spontaneous alignment induces the same alignment in CNTs dispersed into it [7]. Such phenomena are extremely interesting, as only ordered assemblies of CNTs can display relevant properties on a macroscopic scale. Moreover, when an external electrical or magnetic field above the so-called Freedericksz threshold is applied to the LC, the molecules reorient accordingly, and the CNT orientation changes likewise [8]. The mechanism of CNTs reorientation via LCs has been proposed in applications such as electrically or magnetically steered switches [9] and unconventional computing [10].

More generally, LC-CNT mixtures interact in a reciprocal alignment. For instance, CNTs can be aligned by anchoring forces at the LC-CNT interfaces, mainly due to π-π electron stacking between LC molecules and CNTs [11, 12]. Vice-versa, CNTs can induce the formation of short-range pseudo-nematic domains in mixtures containing CNTs in isotropic

Optics EXPRESS

phase LCs [13] (i.e., LCs above the transition temperature from the liquid crystal state to the liquid state), or can induce a helical twist in a non-chiral nematic LC [14].

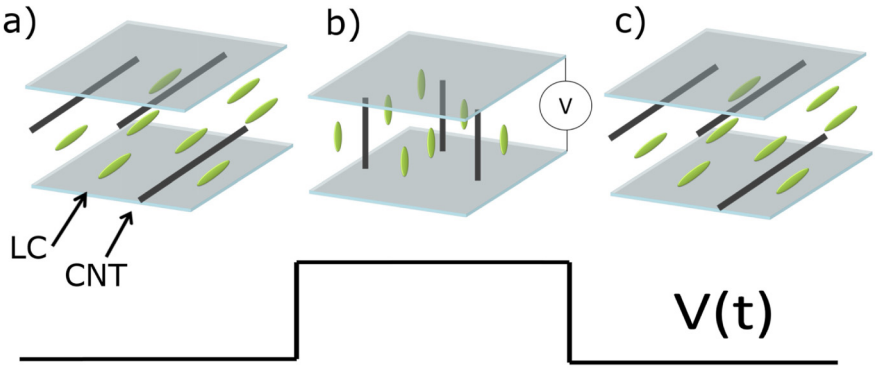

Fig. 1. Effect of an OFF-ON-OFF voltage cycle on the sample LC cell. (a) LC and MWCNTs are originally both planar aligned. (b) Applying voltage above threshold, the positive dielectric anisotropy LC switches to an orientation perpendicular to the plates. (c) When the voltage is switched off, only LC molecules relax to their initial alignment, while CNTs recover only partially.

In this paper, we focus on how the presence of dispersed MWCNTs in a nematic LC mixture can induce short-ranged variations of the molecular director of the LC matrix. In our samples, anchoring forces between LC molecules and cell surface impose a *planar* (or *homogeneous)* alignment to the LC-MWCNT dispersion, meaning that the director ***n*** lies on the plane of the cell plates [Fig. 1(a)]. This alignment can be modified applying electric fields above the Freedericksz threshold. The inner surfaces of the plates are coated with a transparent electrode (indium-tin oxide, ITO), allowing the application of electric fields perpendicular to the plates. If the LC has a positive dielectric anisotropy, the external electric field reorients molecules from planar to *homeotropic* alignment, i.e. with ***n*** perpendicular to the electrode plates. MWCNTs follow the same behavior thanks to the interaction with the LC molecules, resulting in a complete alignment of the whole LC-MWCNT dispersion [Fig. 1(b)]. Once the voltage is switched off, LC molecules relax to the initial planar configuration. Several works have showed how well the dispersed SWCNTs follow the LC relaxation [15]. In a recent work [16], it was found out that MWCNTs only partially recover their original orientation [Fig. 1(c)]. Such experimental studies were based on conductivity measurements and polarized optical microscopy [16]. The phenomenon was ascribed to the strong interaction between MWCNTs and the surface, as well as to the larger inertia of MWCNTs with respect to single walled CNTs.

In this work, we shed light on the effect on the LC orientation of two competing effects: (i) the anchoring forces that induce the planar alignment due to glass-ITO surface functionalization; and (ii) the chemical interaction with the CNTs, which distorts the LC director orientation in close proximity to the nanotube. Under their influence, the LC director undertakes a peculiar pattern in a short-ranged volume surrounding the MWCNT. This persists as topological defect after turning off the electric field since the nanotube does not recover the original state.

2. Results and discussion

2.1 Topological defect formation

Our cells are made of two dissimilar plates. One of the plates is a 0.7 mm-thick ITO-coated glass plate (Glasstone), and the other an ITO-coated 100 μm-thick coverslip. The polyimide mixture used as alignment substrate is deposited on the glasses by spin coating; then glasses

Optics EXPRESS

are rubbed with a velvet cloth to obtain the desired planar alignment. The sandwiched cells, having a gap of 12 μm, were infiltrated by capillarity with the LC-MWCNT mixture.

The LC used is the nematic mixture MLC-6290-000 (Merck). It has positive dielectric anisotropy, with an optical birefringence $\Delta n = 0.12$ at 589 nm and a clearing point at 110 °C, therefore providing an ample nematic-phase temperature range. The LC mixture is doped with MWCNTs (Sigma-Aldrich) with an outer tube diameter of 6-9 nm and a length of about 5 μm. The mixture has an approximate concentration of 0.01 wt%. It is obtained introducing in the LC an adequate amount of a solution of MWCNT diluted in toluene (0.1 wt%). This procedure, coupled with sonication, improves the nanoparticles' dispersion, notoriously hindered by strong attractive van der Waals interactions between individual nanotubes.

Accurate information on the 3*D* spatial arrangement of the MWCNT particles and LC matrix was determined through confocal Raman micro-spectroscopy scanning as clearly discussed later. In the first place, Raman microscopy allowed us verifying the MWCNTs to be formed by sub-wavelength particles (either isolated nanotubes or small bundles). Intensity of the Raman marker bands of MWCNTs was used to ascertain approximated quantity of MWCNTs. We focused further attention only onto spots showing minimal Raman intensity, corresponding to the smallest MWCNTs bundles.

We preliminarily verified global information on the spatial distribution of the LC far from the nanotubes. LCs reorient towards the homeotropic alignment according to the electric field direction. However, in close proximity to the polyimide layer the molecules retain planar alignment regardless of field intensity. A continuous reorientation profile results with maximum alignment along the electric field in the central region of the sandwiched cell. The higher the field, the larger the thickness of such central region. As demonstrated in our previous work on negative anisotropic dielectric mixtures with planar alignment, single-walled CNTs can reorient along the vertical direction not only because they follow the LC matrix reorientation but also thanks to their intrinsic, independent interaction with the external electric field [17].

We found this to occur in MWCNTs as well. In the case under study ($\Delta\varepsilon > 0$), both concurrent interactions additively increase the efficiency of nanotubes reorientation along the field direction. Upon relaxation of the external field, the MWCNTs nearly recover the original direction under guidance of the LC matrix, unless a relatively high voltage is applied.

In this work, we limit our discussion to the distribution of the LC molecules around the topological defect produced by the application of a high driving voltage. The persistent MWCNT reorientation was induced by applying a driving sine wave voltage at 10 kHz for about one hour. We chose this modulation frequency to avoid the formation of double-layer due to the presence of ions in our mixtures. The amplitude voltage was of 20 V, i.e. well above the Freedericksz transition. Both intensity and application time were chosen in order to optimize the formation of stable LC structures around the vertically aligned CNTs after field release. The topological defects, once formed, stay unchanged over a span of several weeks if the cell does not undergo any electrical or mechanical stress. Indeed, we have observed that the application of a high intensity, low frequency voltage (20 V at 100 Hz) can effectively erase such structures. We ascribed this phenomenon to the ions flow, more effective at low frequencies, which can drive molecular displacements around the nanotube, eventually destabilizing the stacked vertical orientation of MWCNTs. Further measurements are needed to get a deeper insight on this phenomenon. Upon finishing the field application, the MWCNTs vigorously move around their positions. Once the low frequency field is released, MWCNTs follow again the LC matrix orientation, so the cell recovers the initial state [Fig. 1(a)].

2.2 Ellipsometry

Ellipsometry is a non-contact and non-destructive optical technique that analyzes the changes in the polarization state of a light beam upon reflection from (or transmission through) a

Optics EXPRESS

sample. The ellipsometer used in this work is the variable angle spectroscopic ellipsometer (V-VASE) *W1-01* (J.A. Woollam Co. Inc.), which permits the automated acquisition of data, varying both the wavelength λ of the incident light and its angle of incidence α. This technique can be used on LC slabs to extrapolate, using a complex inversion procedure on the experimental data, macroscopic optical parameters such as the anisotropic refractive index and extinction coefficient, but also the orientation of the optical axis [18,19]. Obtaining quantitative information on the parameters requires setting an optical model of the sample under study, then a fit procedure matching model-generated data with experimental ones.

We characterized the LC-MWCNT cells in two states: before and after applying the switching voltage, i.e. without and with topological defects. Since defects change local orientation of LC molecules, they are visible under polarized microscopy; we expected to observe a difference in the complex refractive index and optical axis tilt θ with respect to the cell plane. Note that the obtained parameters were averaged over an area of about 3 mm^2 (beam diameter = 1 mm).

Cells under study were oriented with rubbing direction orthogonal to the incidence plane. We used two data acquisition modes: 1) general ellipsometry (GE) measurements for wavelength $\lambda = 500\,nm$ and for angle of incidence ranging from −60 to 15 degree and 2) transmittance measurements for normally incident p- and s-polarized light in the wavelength range from 400 nm to 1600 nm. The former measurements give ellipsometric parameters related to the ratios of the Jones matrix elements: $\Psi = \arctan(|t_{pp}|/|t_{ss}|)$, $\Psi_{ps} = \arctan(|t_{ps}|/|t_{pp}|)$, $\Psi_{sp} = \arctan(|t_{sp}|/|t_{ss}|)$. Here Jones matrix describes transmission of light through the sample as follows:

$$\begin{bmatrix} B_p \\ B_s \end{bmatrix} = \begin{bmatrix} t_{pp} & t_{sp} \\ t_{ps} & t_{ss} \end{bmatrix} \begin{bmatrix} A_p \\ A_s \end{bmatrix}$$

where A_p, A_s and B_p, B_s are the p- and s-components of the incident and transmitted electric field, respectively. At a chosen sample orientation, GE measurements provide maximum sensitivity to the tilt angle [18]. The latter mainly give information about dispersion of anisotropic refractive index and about both polarization and spectral dependences of light attenuation by the sample. In Fig. 2 the experimental and simulated data for Ψ and Ψ_{sp} parameters are presented versus angle of incidence.

All experimental data were fitted using the appropriate optical model of the cell. Since the comprehensive optical model contains too many unknown parameters, namely refractive indices and thickness of each layer, the glass substrate, ITO and polyimide alignment layers were first characterized using the special samples. The obtained optical constants of those layers were fixed in the optical model of the cell. Cell gap was fixed at nominal value 12 μm.

Notice that the off diagonal nonzero elements appear for nonzero tilt and incidence angles. Moreover, they increase with tilt and incidence angle for small α. However, for $\alpha > 40°$, Ψ_{sp} decreases and tends to another minimum at a value α^* for which ordinary and extraordinary beams have phase difference 2π after passing through the cell [Fig. 2]. The tilt values obtained from the fit are $3.9° \pm 0.3°$ and $4.8° \pm 0.3°$, respectively before and after application of the external field. Note that these are effective values corresponding to the integral of polarization transformation through the cell gap. The observed small increment of tilt angle is ascribed to the small number of defects appeared in the gap volume caused by vertically aligned MWCNTs.

Ψ parameter becomes higher after application of an external field indicating growth of the ratio $|t_{pp}|/|t_{ss}|$. This is in agreement with transmittance measurements [Fig. 3].

Optics EXPRESS

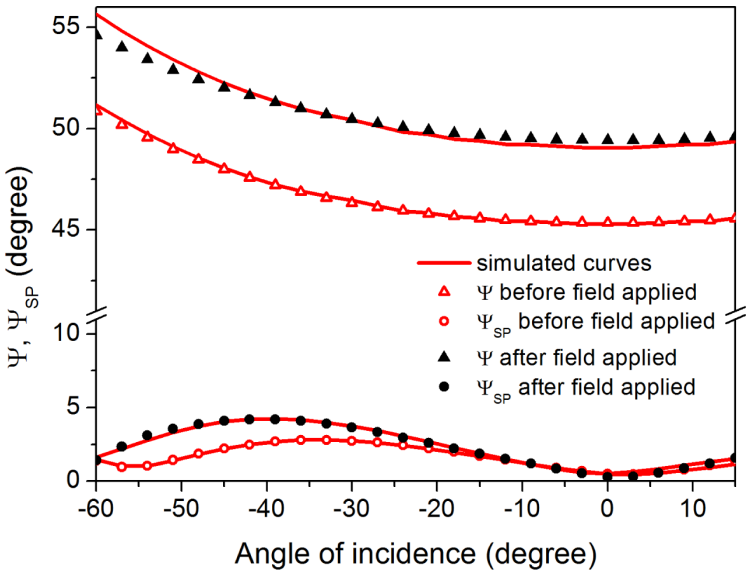

Fig. 2. Experimental (symbols) and simulated (lines) Ψ and Ψ_{sp} parameters, before and after the application of an external field.

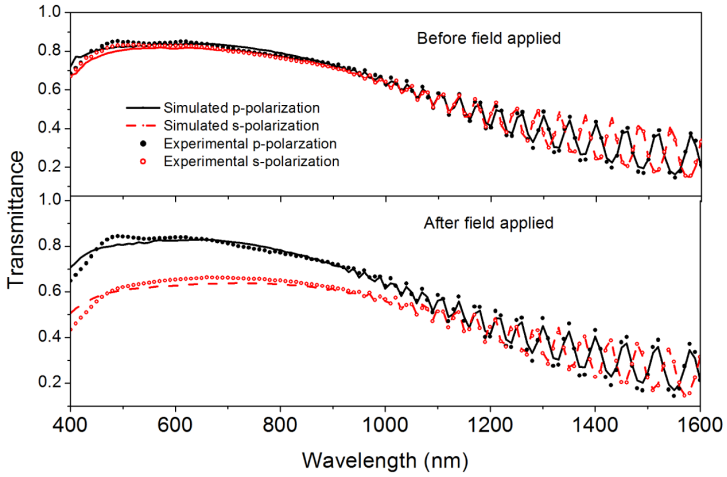

Fig. 3. Experimental and simulated data for transmittance of the p- and s-polarized light, before and after the application of the high intensity external field.

It is evident that the application of an electric field results in a significant decrease of the transmitted light only for the s-polarized light, and mainly in the visible range. In order to describe the observed light attenuation by the model, we introduced a pseudo extinction coefficient κ to the formula for the complex refractive index of the LC-WMCNT mixture as follows: $N = n + ik$. With no field, the fit procedure gives for the two polarizations $k_p = 0.006$ and $k_s = 0.0006$ at $\lambda = 500\,nm$. After application of the field, $k_p = 0.007$ and $k_s = 0.0015$. The k_s attenuation is caused by light scattering and not by absorption. Nevertheless, the pseudo parameter k can be used for formal mathematical description of the observed losses and for obtaining a good fit of all the experimental data (see Fig. 2 and Fig. 3) using the same optical model. In our sample, we verified that losses are due to light scattering from the topological defects. In fact, the light intensity collected immediately before and after the sample is substantially unchanged, while the transmitted signal decreases with the detector-sample

Optics EXPRESS

distance. Moreover, the defects scatter more for s-polarized light, i.e. parallel to the direction of rubbing. Therefore, an anisotropic orientation of the LC matrix is expected around the vertically aligned MWCNT that induces the defect.

2.3 Raman spectroscopy

Raman spectroscopy is commonly used to obtain the vibrational fingerprint of molecular species by which they can be identified [20]. Moreover, given the anisotropic character of molecular polarizabilities, Raman spectroscopy also provides a powerful tool to image orientational order of molecules since the angle formed between the probing light polarization and the analyzed molecules affects the Raman signal's intensity. This has been demonstrated for both LCs [21,22] and CNTs [23].

A detailed analysis of the LC behavior around MWCNTs after defect formation was performed with Raman spectroscopy. To this end, we used the system *WiTec alpha300* in an inverted micro-Raman configuration, whose description is reported in [24]. It employs a confocal microscope setup to acquire information locally resolved in three dimensions, enabling lateral and depth profiling of samples. By using a 60X objective, the spatial resolution is of ~0.4 μm in the transverse *x*-*y* plane and of ~2.6 μm along the axial *z* direction. The measurements were performed with an excitation wavelength of 532 nm at laser powers of a few mW, in order to prevent any optical trapping or excessive heating of the LC matrix, which could affect the director structure. In Fig. 4, we report Raman spectra of the LC in different configurations, obtained in a sample without MWCNT dispersion. This spectra were also found in sample with MWCN, at distance of about 8-10 μm from the induced defects center.

The most significant vibrational modes of liquid crystalline materials are the symmetric and asymmetric stretching of CH_2 bands at 2852 and 2930 cm^{-1} respectively, the CN symmetric stretching band at 2220 cm^{-1} and the CC (aromatic ring) vibration band at 1610 cm^{-1}. This is compatible with the general structure of a rod-like molecule consisting of a rigid core of aromatic rings, a flexible aliphatic tail and one or more polar groups. These three bands have different orientation with respect to the liquid crystal chain: CC and CN are parallel to it, whereas CH_2 is perpendicular. In our experiment, we used two different configurations to show how the intensity of these modes depends on the LC's orientation. In Fig. 4(a), no electric field is applied and LC is in planar alignment. The cell surface is located in the *x*-*y* plane, while the laser light travels along the *z* axis and is linearly polarized. along the rubbing direction, so $\mathbf{P}\|\mathbf{n}$. The aromatic ring and the CN bonds give a strong Raman signal. Conversely, the CH_2 bonds from the long hydrocarbon tail are orthogonal to the incident polarization and their correspondent signals are low.

The situation is reversed whenever the LC molecular axis is orthogonal to the incident polarization [Fig. 4(b)]. This may happen if the cell is rotated around the *z* axis by 90°, or if a driving voltage is applied. In the former case the molecules lay along the *y* axis, while in the latter case their orientation changes from planar to homeotropic, so that the molecular director tends to align to the *z* axis. In both configurations, the intensity of the CC and CN bands largely decreases while the intensity of the CH_2 band increases.

Unlike LC molecules, MWCNTs show a weak Raman response, easily masked by the LC signal. Focusing the laser near the bottom glass where LC signal is weaker, the. MWCNT Raman contribution was clearly identified and characterized by several bands among which the most prominent is at 1580 cm^{-1}. The position of maximum integrated Raman intensity around 1580 cm^{-1}, i.e. the CNT's position, defines the defect center. Around this point, one can start the scanning for determining the LC configuration. To this end, we carried out a raster scan recording 50 lines with 50 spectra per line over a surface of 100 μm^2 around the defect, at different height above the lower cell's wall. Raman intensity of the bottom glass slide (914 cm^{-1}) was used to mark the origin of the *z*-coordinate system. From each spectrum,

Optics EXPRESS

we extracted the area under the peaks corresponding to the CC (1560 – 1650 cm^{-1}), CN (2150 – 2280 cm^{-1}) and CH_2 (2800 – 3000cm^{-1}) stretching bands of LC. The areas were then plotted assigning a color to integrated intensity, thus reconstructing a 2*D* Raman imaging map of the area.

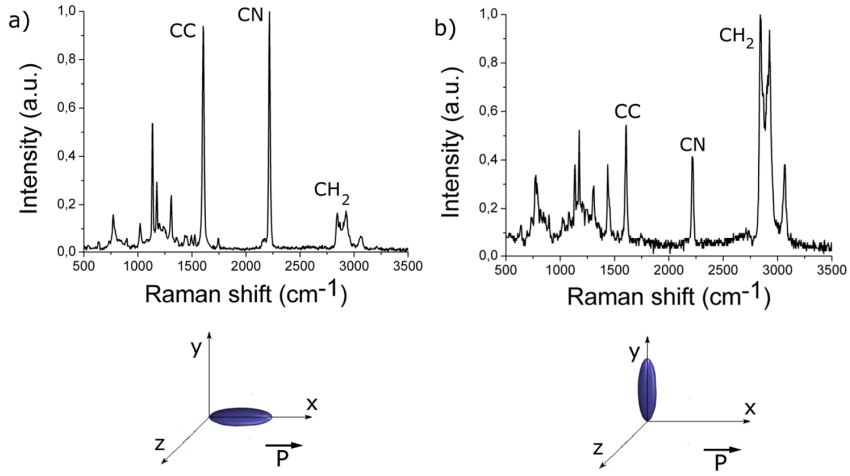

Fig. 4. Representative LC spectra in different configurations: the incident light is polarized along the *x* axis, while the LC molecular director may lay along it (a), or orthogonal (b). The intensities are normalized to the highest peak. Depending on the orientation of the LC molecules, the aromatic ring CC (1610 cm^{-1}), cyano group CN (2220 cm^{-1}), and CH_2 (2800-3000 cm^{-1}) stretching modes change their intensity.

Figure 5(a) reports the maps of the CN group, acquired for different heights in a configuration with the cell rubbing direction orthogonal to the incident polarization. The height $z = 0$ is adjacent to the cell surface, and increases as the objective lens is moved towards the cell center. This depth analysis can be used to confirm that the MWCNTs are aligned vertically even after the field is switched off. The weakness of the MWCNTs Raman signal and the limit of our resolution make it impossible to obtain satisfactory maps of a nanotube Raman peak. However, as said before, a detailed analysis can ascertain the presence of MWCNT signal at the center of the studied topological defects. In the reported maps, its position corresponds to the center of the inner zone (in red), where, as clearly explained later, the signal from the LC's CN group is stronger. An evaluation of the displacement of the central zone in the *x*-*y* plane, when moving vertically, allowed us to estimate a tilt $\alpha \sim 8°$ between the MWCNT axis and the *z*-axis [Fig. 5(a)].

Optics EXPRESS

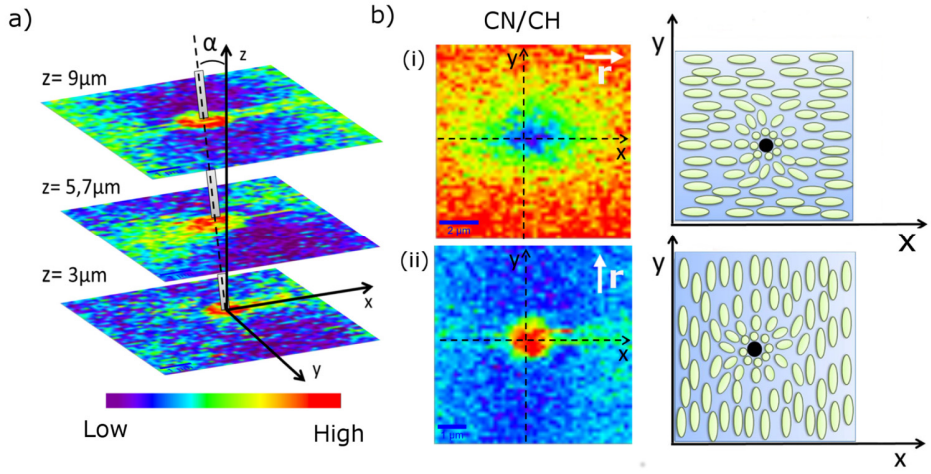

Fig. 5. (a) Integrated intensity maps of CN band of LC at different depths; the central zone corresponds to the MWCNT presence. (b) Maps of the ratio between the integrated intensity of the CN and CH_2 bands over a surface of 100 μm^2 around a defect (central point). The cell is in two configurations: with the rubbing direction parallel to *x*-axis (i) and along *y*-axis (ii). Incident polarization is parallel to the *x*-axis. The beam, having a confocal depth of 2.6 μm, is focused nearly 6 μm above the bottom glass. Right pictures depict a sketch of the proposed corresponding LC director distribution around the defect (the black dot indicates the vertically aligned MWCNT).

After checking the MWCNT orientation, we studied the arrangement of the LC molecules surrounding it. As said before, the peak intensities in the Raman spectrum depend on the molecular orientation with respect to the incident light polarization. In particular, when the LC molecules are parallel to the polarization, the CC and CN peaks have higher intensities than the CH_2 peak [Fig. 4(a)]. The opposite is true whenever the LC molecules are orthogonal to the light polarization. Therefore, it is possible to study the molecular director configuration around the MWCNTs by mapping the relative intensity of the two molecular vibrations. In particular, to highlight the information on the relative peak intensities, we have plotted the ratio between the values of the area under the CN and CH_2 peaks. In the following, we will refer to it as CC/CH_2. Reporting any other ratio (CC/CH_2 or CC/CN) would be superfluous, as the CC and CN bands show the same behavior when rotating the LC molecules.

We acquired the maps with the cell in two configurations, with the rubbing direction parallel and orthogonal to the incident polarization **P** [Fig. 5(b)]. In the first case [Fig. 5(b-i)], the signal from the CN group is stronger than the signal from the CH_2, so $CC/CH_2 > 1$. This means that the LC molecules are never oriented completely orthogonally to the incident polarization. However, the ratio intensity is higher far from the defect, and decreases toward the MWCNT (black dot in the sketch). Since we are analyzing a ratio, we can be sure that the signal decreases only due to a LC reorientation, neglecting any other effect. In particular, where the signal is weak, the molecules are less aligned along light polarization.

In order to speculate how the molecular director changes, we start by fixing two constraints: (i) the LC director, far from the CNTs, tends to the planar orientation imposed by the alignment layer; (ii) LC molecules immediately surrounding the nanotubes are aligned along the CNT axis by π-π electron stacking.

Let us consider the *x* axis, passing through the defect center in Fig. 5(b-i): along this direction the signal behavior and the two constraints are compatible with a continuous rotation of the molecular director in the *x-z* plane. Also in the orthogonal direction the ratio decreases, so the molecules are less aligned along the polarization when close to the CNT. The constraint at the nanotube surface again suggests that the molecules must rotate out of the *x-y* plane. However, a possible contribution of the rotation in the *x-y* plane cannot be

Optics EXPRESS

excluded. It should be noticed that the LC molecular pattern is not symmetrical. The distortion from the planar behavior is astigmatic and occurs on a larger length scale in the direction of the rubbing. This is another consequence of the competition between the anchoring forces to the alignment layer and to the nanotubes surfaces. In fact, when approaching the nanotube along the rubbing direction the LC director experiences a bend deformation. Along the orthogonal direction, it undergoes in addition a twist deformation, so that the overall distortion results more energetically consuming as compared with the first case. As a result, the nanotube's influence on LC director configuration propagates for longer distance along the rubbing direction than along the perpendicular one.

When the cell is rotated so that incident polarization and rubbing direction are orthogonal, the intensity distribution of the ratio changes [Fig. 5(b-ii)], and different information can be extracted. The most significant feature is that the intensity of the CC and CN peaks increase in the central zone. Since the CN peak is not influenced by any possible Raman signal from the MWCNT, the observed variations are related to a LC reorientation. In particular, far from the MWCNT, the signal from the CN is weaker than that from the CH_2 group, so that $0 < CC/CH_2 < 1$. This is compatible with the previously suggested orientation of the LC molecules along the rubbing (now in the y axis direction) or with a tilt in the y-z plane towards the nanotube. In both configurations, the molecules result orthogonal to the polarization **P**.

However in the central zone, in red in Fig. 5(b-ii), the CN Raman signal becomes higher than that from CH_2 . Thus, the ratio has values $CC/CH_2 > 1$. It means that the LC molecules around the MWCNT acquire a significant component along the polarization. This phenomenon cannot be explained only by the slight tilt of the nanorod respect to the z-axis. We ascribe it to the peculiar nature of the chemical bonds between MWCNT and LC. The π-π stacking, binding MWCNT and LC, forces the LC molecules to align along a preferred direction on the nanotube's surface, which depends on the chirality of the outer layer of the MWCNT. Notice that this effect is much more localized in the map reported in Fig. 5(b-i): in a restricted area around the MWCNT the LC director is rotated following the surface. Moving far from the MWCNT, the nanotube influence decreases causing only a small tilt in the LC, which eventually returns to the planar alignment.

The maps of the defects were also collected at different heights along the z-direction, so that we could observe the changes in the LC structure in 3*D*. In Fig. 6, the results obtained plotting the area under the CN aromatic ring band are reported. The cell is oriented with the rubbing direction along the light polarization. The height $z = 0$ is adjacent to the cell surface and shows the presence of localized carbonaceous impurities other than the MWCNT. The other maps were acquired moving the objective lens towards the cell center. The darker zone in each figure, corresponding to the presence of the MWCNT, is located approximately in the same (x, y) position although a 1 μm displacement is visible along the z-axis. As seen before, we can thus evaluate the MWCNT tilt respect to the z axis, which is about 6°. Regarding the changes in the LC director, moving from the bottom of the cell towards the central region, the distribution of LC molecules reflects a slower variation of the molecular orientation. This is reasonable as the anchoring force to the alignment layer decreases with distance from the surface [6]. This effect is visible in Fig. 6, in which the maps acquired at higher z values exhibit wider blue-green regions, mirroring an increased MWCNTs influence far from the polyimide layer. We have defined an effective defect area as the region in which the peak intensity is lower than a threshold, fixed at 64% of the maximum. In the maps in Fig. 6, the area perimeter approximately matches the yellow zone. Going from the plane $z = 0$ to the plane $z = 8{,}25$um, the area so defined increase of the 87%.

Optics EXPRESS

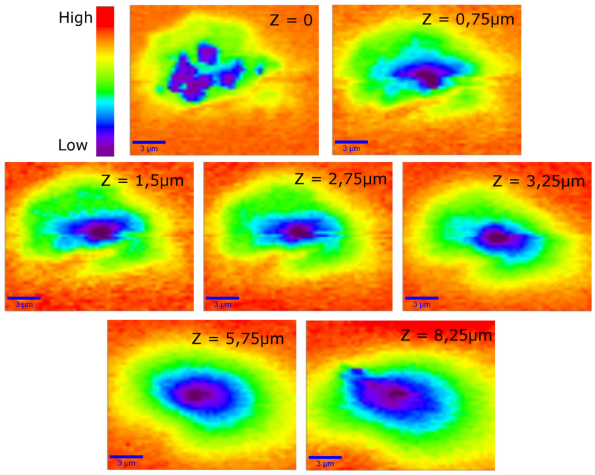

Fig. 6. Raster scans of the integrated intensity of the cyano peak CN acquired at different depths along the cell around the MWCNT.

3. Conclusions

In this work we highlights how the LC-CNT interaction, in concomitance with an adequate choose of cell's configuration, can be exploited to induce the formation of peculiar structures by LC self-assembly. In particular, we show that LC-MWCNTs dispersion exhibit a change in the optical response after the application of a high amplitude-high frequency voltage (20 V at 10 kHz), and a number of topological defects persist after the switch-off of the field.

Ellipsometry measurements reveal small change in the optical axis orientation of the LC-MWCNT mixture after application of voltage, which actually reflect deformations of the LC matrix around MWCNTs. Transmittance measurements showed an anisotropic behavior of the cell, as light polarized along the rubbing direction is scattered more because it experiences a much greater refractive index gradient across the topological defects than orthogonally polarized one according to the defect morphology. Raman sensitivity to the molecular orientation of the liquid crystal allows to determine the spatial distribution of the molecules around the MWCNTs. The results show that the MWCNT's presence strongly affects the structure of LC, notwithstanding the alignment imposed by the cell's surfaces. The final effects is that far from the MWCNTs the LC molecular director is unperturbed, while near them the LC molecules tilt to follow the nanorods orientation. Between these two states, the molecular director changes with continuity.

Our results provide new insight into LC-CNT interaction capability and suggest the possibility to engineer electrically driven liquid crystal patterns pinned by CNTs arrays for scattering devices. Further studies could provide a more detailed analysis of the factors that influence the formation of metastable structures of MWCNTs with vertical alignment (i.e. CNTs concentration, structure, interaction with the external matrix and alignment layer) opening the door to potential applications in bistable devices. For applications in reversible devices, such as externally controlled switches or sensors, this study could instead define the conditions under which a disadvantageous irreversibility can manifest. Moreover, our experimental approach is potentially applicable to graphene sheets or nanoribbons as well as to other nanorod materials.

Acknowledgments

This work has been partially supported by ICT COST Action IC1208 "Integrating devices and materials: a challenge for new instrumentation in ICT" and Spanish Government RETOS Program grant no. TEC2013-47342-C2-R.